Iranian Journal of Medical Physics

ijmp.mums.ac.ir

Evaluation of an Analytical Anisotropic Dose Calculation Algorithm in a Heterogeneous Medium Using *In Vivo* Dosimetry for High-Energy Photon Beams

Yasmina Berkani[1*], Rachid Khelifi[1]

1. Department of Physics, Faculty of Science, Laboratory of Theoretical Physics and Matte Radiation Interaction (LPTHIRM), Saad Dahlab University of Blida, Algeria

A R T I C L E I N F O

Article type:
Original Paper

Article history:
Received: Mar 03, 2021
Accepted: Jun 19, 2021

Keywords:
Radiotherapy
Rib Cage
Diode
Heterogeneity
Anisotropic Analytical Algorithm

A B S T R A C T

Introduction: The calibration process is usually limited to the depth of maximum energy. This study aimed to determine the depth dose in a heterogeneous medium using diodes and to evaluate a dose calculation algorithm.

Material and Methods: Measurements were done at three depths (4, 8, and 12 cm) using ten QED^{TM} diodes on heterogeneous phantoms (HPH), composed of poly(methyl methacrylate) (PMMA) and expanded polystyrene, roughly simulating the rib cage. These phantoms were irradiated with 6-MV and 18-MV photon beams from a Varian linear accelerator by plans calculated by the Eclipse treatment planning system, equipped with the Anisotropic Analytical Algorithm (AAA). The calibration curves were drawn by considering several measurement points in depth by a graphite ionization chamber in the HPH. The diode calibration factor was taken from the curves via interpolation. The measured and calculated values were compared to evaluate the AAA.

Results: Depending on the depth, the deviations between the measurements and calculations predicted by the TPS remained less than 2%. Some measurements had an order of magnitude of nearly 3%. An average deviation of 1.13% was obtained for all measurements, with an average deviation of 0.66% and a standard deviation of 0.80%. The upper bound of the confidence interval was 1.41%.

Conclusion: The deviations obtained in this study remained within the recommended standard range for validation of a dose calculation algorithm in a heterogeneous medium. The calibration method based on dose profiles provided further information about the dose in a heterogeneous medium, based on a single diode reading.

► *Please cite this article as:*
Berkani Y, Khelifi R. Evaluation of an Analytical Anisotropic Dose Calculation Algorithm in a Heterogeneous Medium Using *In Vivo* Dosimetry for High-Energy Photon Beams. Iran J Med Phys 2021; 19: 22-30. 10.22038/ijmp.2020.46457.1739.

Introduction

In radiotherapy, determining the dose at a specific point in a heterogeneous medium, which reflects the tissue architecture, is a real challenge for medical physicists. Validation of a dose calculation algorithm in a treatment planning system (TPS) requires verification in heterogeneous devices. The International Atomic Energy Agency (IAEA) technical report series TRS-430 recommends the use of cork sheets with a low density for simulation [1]. Besides, control of deviation between calculations and measurements of absolute doses has become an interesting research topic. Therefore, evaluation of other density organs, such as the lungs and bones, seems necessary, because of their effect on dose distribution [2].

In the presence of heterogeneity, a TPS tends to correct the dose calculations by converting them to homogeneous calculations similar to those in a water-equivalent medium; this influences the precision of calculations, especially for correction of scattered radiation [3]. Also, in several TPSs, the accuracy of calculation becomes more significant under relatively simple geometric conditions [3], which explains the errors encountered in the past [4-9]. The Anisotropic Analytical Algorithm (AAA) is an algorithm that considers the path of electron contamination. Based on the Monte Carlo (MC) simulations, it is necessary to carry out tests on heterogeneous phantoms for absolute dose measurements. Therefore, determining the dose at a point enables risk assessment in the affected area if it is a region to be spared; it also facilitates the assessment of the optimal area coverage for treatment when it is the target volume. The present study aimed to develop a method for calibrating diodes, depending on the diode depth, by conducting experiments in heterogeneous phantoms.

The conventional methods of diode calibration are based on the input and output doses. The precision of these methods depends on the installation and corrective factors [10-13]. However, recently, only

**Corresponding Author:* Tel: +213 558808914; Email: berkani.yasmina@yahoo.fr

reading of the input dose has been considered, as this dose is often limited to the depth of maximum beam energy (d_{max}). The formula is complex and incorporates the tissue phantom ratio (TPR) [14]. In this study, we focused on determining the absolute dose profiles according to the TRS-398 code [15] to not only obtain a single calibration factor, but also plot the calibration curves.

Materials and Methods

The measurements and calculations in the experimental section of this study were carried out at the Radiotherapy Department of Anti-Cancer Center of Blida, Algeria.

Diodes and physical characteristics

The major measuring instruments used in this study were the QED^{TM} diodes (Sun Nuclear), the physical characteristics of which have been described in a previous study [16]. The calibration factor, F_{cal} (Figure 1), was defined as the ratio of the dose (D_W) at source-skin distance (SSD)+d_{max} measured by the reference detector to the reading R of diode at SSD (cm), based on Equation 1 [16]:

$$F_{cal} = \frac{D_W(100+d_{max})}{R(100)} \quad (1)$$

This factor is measured at the maximum energy depth. It is checked periodically by monitoring the diode response variations as compared to the cumulative dose [17]. It was corrected by other factors that might influence the results, including the SSD, field size, dose rate, and beam obliquity.

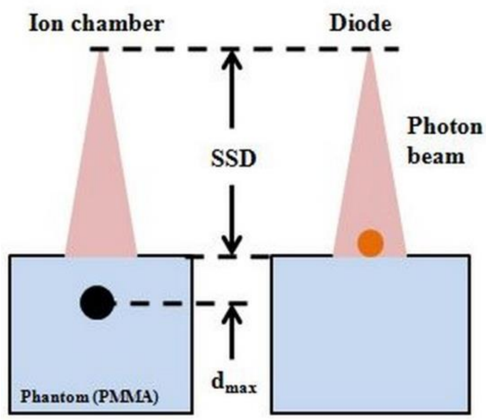

Figure 1. The diode calibration setup in a homogeneous phantom. The first step was carried out with the ionization chamber placed at maximum depth. In the second step, reading of the diode placed at the surface of the same phantom was done.

It is often recommended to use a single factor and monitor it over time while considering the corrective factors [13, 18-20]. Depending on the measurement conditions, these factors can influence the results and cause errors if they are ignored, especially if the patient shows respiratory variations (e.g., variations in the corrective factor related to SSD) [14]. These factors must be also considered if the measurement conditions differ from the geometric calibration conditions [14].

In this study, five diodes (D1-6, D2-6, D3-6, D4-6, and D5-6) were used in the 6-12 MV energy range, and five others (D1-18, D2-18, D3-18, D4-18, and D5-18) were used in the energy range of 15-25 MV. These diodes were labeled according to the energy used and the associated channel. Moreover, it was found that the reading of diodes is fairly stable with respect to the signal linearity and reproducibility. As for the corrective factors, they were ignored due to the similarity of geometrical conditions for calibration and measurements.

AAA algorithm

The AAA algorithm is an Eclipse (Varian) TPS algorithm; the version used in this study was v. 13.6, as described in previous studies [21, 22]. It is an improved pencil beam algorithm, based on a convolution/superposition model. The beam kernel is drawn from the MC calculations and adjusted to fit the commissioning measurements. The correction of heterogeneities considers the scattered kernels of photons and electrons, depending on the distribution of the medium electron density [23].

Measurement strategy

Commonly, homogeneous water-equivalent phantoms are used for the calibration of diodes. In this study, we aimed to examine the behavior of depth-dose profiles of high-energy photon beams in a heterogeneous medium, composed of plastics poly(methyl methacrylate) (PMMA) plates and expanded polystyrene sheets. Although the total thickness can be converted to a water-equivalent thickness, we maintained this type of plate arrangement for calibration to approximate the tissue architecture of the rib cage with a tumor in the medium with a density similar to the lungs.

Besides, a preliminary study was carried out with a standard calibration. Comparison of calculations and the results obtained from patients for head, neck, and prostate localizations indicated the expected tolerable levels; however, significant deviations were found on a anthropomorphic phantom for thoracic localizations. Once calibration was carried out in a heterogeneous medium, an experimental study was performed to compare the measurements with TPS calculations to determine if the dose calculation algorithm was necessary. The phantoms were made of blocks of expanded polystyrene, where a small PMMA insert was introduced to simulate a small tumor in the rib cage. This arrangement was selected to carry out measurements at depths other than that of calibration.

Determination of absolute dose profiles in a heterogeneous medium

The first part of this study focused on the measurement of absolute doses by a reference detector.

Three dose profiles at SSD of 100 cm for each energy level (namely, 6 MV and 18 MV), in parallel to a beam with dimensions of 10×10 cm^2 from a Varian 2100C linear accelerator, were acquired through a graphite ionization chamber with a volume of 0.6 cc (Farmer NE2571, Nuclear Enterprise) and a UNIDOS electrometer (PTW). Measurements were carried out in a phantom made of PMMA plates with a density of 1.18 g/cm^3 and low-density expanded polystyrene plates (0.15, 0.20, and 0.25 g/cm^3).

To roughly simulate the rib cage, the PMMA plates, with a total thickness of 3 cm, were placed in the upper and lower parts of the phantoms; besides, expanded polystyrene plates were included. For dose measurements, a PMMA plate with a hole to introduce the Farmer chamber was placed at different depths (between the expanded polystyrene plates) to measure the depth dose (Figure 2). Several points were considered for each phantom (three phantoms). For two energies and each depth, five readings were taken and averaged (Rav). The dose measured with the ionization chamber (D_{IC}) was obtained based on the calibration factor N. The formula is presented in Equation 2:

$$D_{IC} = R_{av}.N.K_{TP}.K_{Pol}.K_S.K_Q \ \ (mGy) \quad (2)$$

where K_{TP} is the corrective factor related to temperature and pressure, K_{POL} is the polarization corrective factor, K_S is the recombination corrective factor, and K_Q is the corrective factor of chamber response between the reference quality beam and the used quality beam.

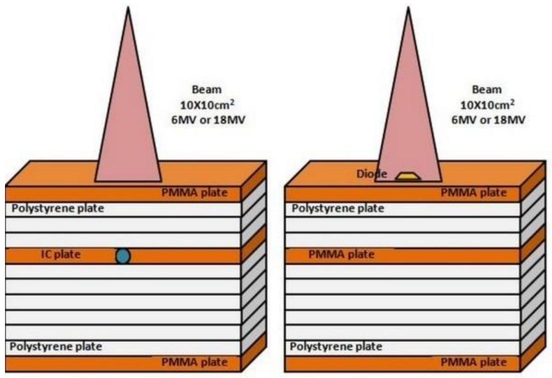

Figure 2. The experimental device for determining the calibration curves. The first part was carried out with an ionization chamber and its plate (IC plate). In the second part, the plate was replaced by a homogeneous PMMA plate without holes, and measurements were done by diodes.

Determination of calibration curves

Before the diodes could be used in heterogeneous phantoms, the calibration curves were drawn. The described devices were used for measurements, with diodes placed on the surface. The plate of the ionization chamber with a hole was replaced by a full PMMA plate (Figure 2). The calibration factor $F_{Cal,Z}$ was determined at each depth of measurement relative to the D_{IC} dose profile (Equation 3):

$$F_{cal,Z} = \frac{D_{IC}}{R} \quad (3)$$

where R is the reading taken from the diode on the surface.

Heterogeneous phantom measurements

Heterogeneous phantoms (three types) with a parallelepiped geometry and two densities were fabricated (Figure 3). We focused on tumors located in the rib cage in this study. To evaluate the dose calculation algorithm, cylindrical PMMA inserts with a diameter of 2 cm, intended to simulate small tumors, were introduced at different depths (7, 11, and 15 cm). The phantoms were scanned, and CT image slices were imported from the scanner to the TPS. A dose calculation was performed at the center of inserts for a field of 10×10 cm^2 at SSD of 100 cm for two energy levels of 6 MV and 18 MV (Figure 4). The calculated plans were irradiated under the accelerator. The dose at the center of inserts was measured from the readings of diode R_D deposited on the surface of the phantoms (Figure 5). The measured dose (D_M) was calculated by Equation 4:

$$D_M(mGy) = R_D \times F_{Cal,Z} \quad (4)$$

Where the calibration factor $F_{Cal,Z}$ is taken from the calibration curves by interpolation for each depth z.

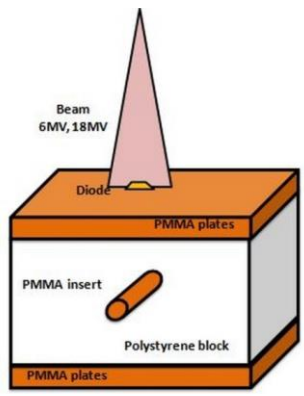

Figure 3. Measurements in a heterogeneous phantom. Cylindrical PMMA inserts were introduced into polystyrene blocks to measure the center dose and compare it to the AAA calculation.

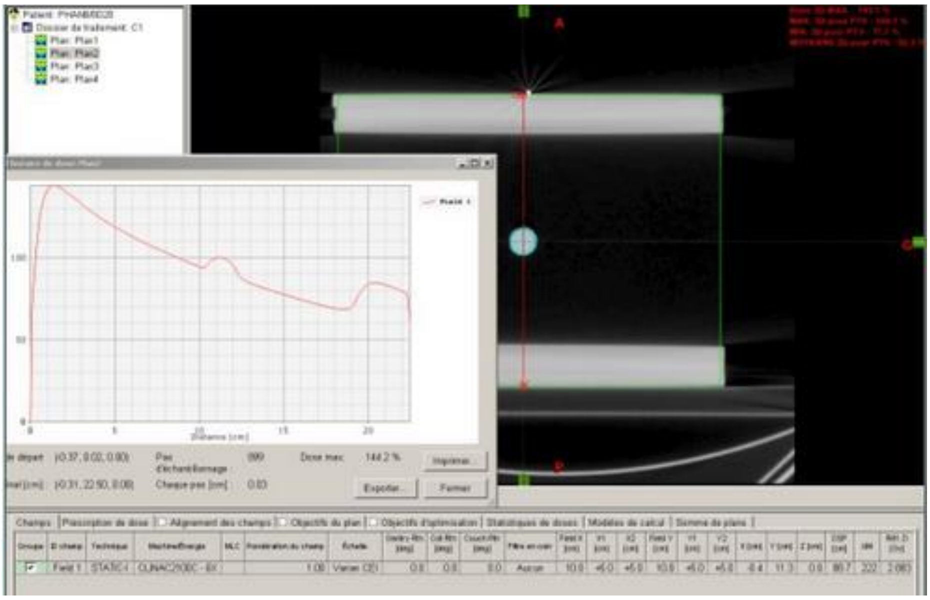

Figure 4. The AAA dose calculation at the center of the PMMA insert.

Figure 5. Irradiation of phantoms under the linear accelerator.

Algorithm assessment method

The algorithm was evaluated by calculating the deviation between the measured dose D_M and the calculated dose of TPS, D_C, at the center of inserts, according to Equation 5:

$$\delta\ (\%) = \left(\frac{D_C - D_M}{D_M}\right) \times 100 \qquad (5)$$

In a region with a low gradient dose, in the presence of heterogeneity, a dose difference of 3% between the calculation and measurement was considered acceptable to validate the dose calculation algorithm. For more complex geometries, a deviation of 4% can be obtained [24].

Statistical analysis

Some statistics related to deviations and measured doses of 1 Gy irradiation were determined, including the average set of measurement points, average deviation, standard deviation, and confidence intervals at 95%, 99%, and 99.9%. Histograms, as a function of density and depth of measurements with a normal distribution, were also plotted.

Results

Six dose profiles were plotted as a function of depth Z. Each thickness, $Z_{h,I}$, relative to the density ρ_i of materials, was converted to a water-equivalent thickness, according to Equation 6:

$$Z = \sum Z_{h,i} \times \rho_i \qquad (6)$$

The curves (Figure 6) were separated according to the three densities. Each diagram shows the relationship between the dose measured by the ionization chamber at two different energies per specific depth. For similar depths, 30 calibration curves were drawn for each diode (Figure 7). The AAA evaluation was carried out using measurements on heterogeneous phantoms. A total of 90 measurements were carried out (Table 1). Some statistical parameters were determined (Table 2), and histograms were plotted (Figure 8), highlighting deviations as a function of energy, density, and depth. A normal probability distribution is also presented in Figure 9.

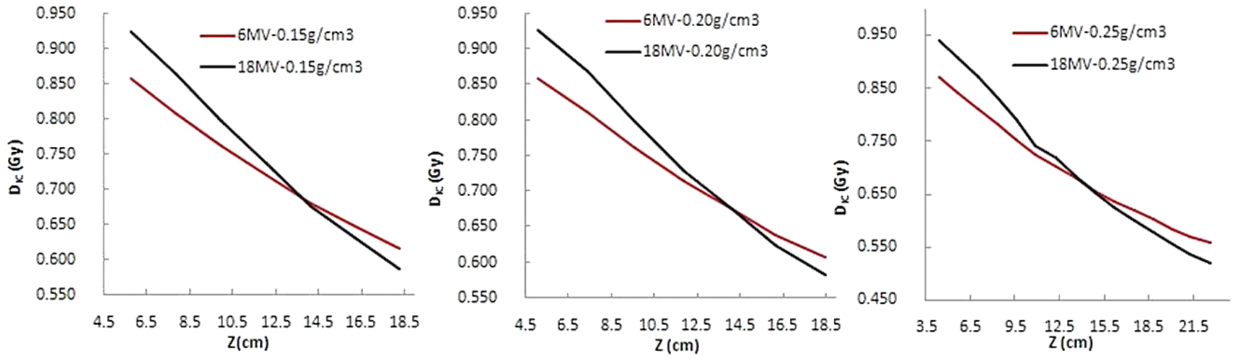

Figure 6. Dose profiles for 6-MV and 18-MV energies. Depending on density, the 6-MV beam accumulated a higher dose at the end of the path (13.7 cm for 0.15 g/cm^3; 14.1 cm for 0.20 g/cm^3; and 14.3 cm for 0.25 g/cm^3) compared to the 18-MV beam, highlighting the backscattered radiation.

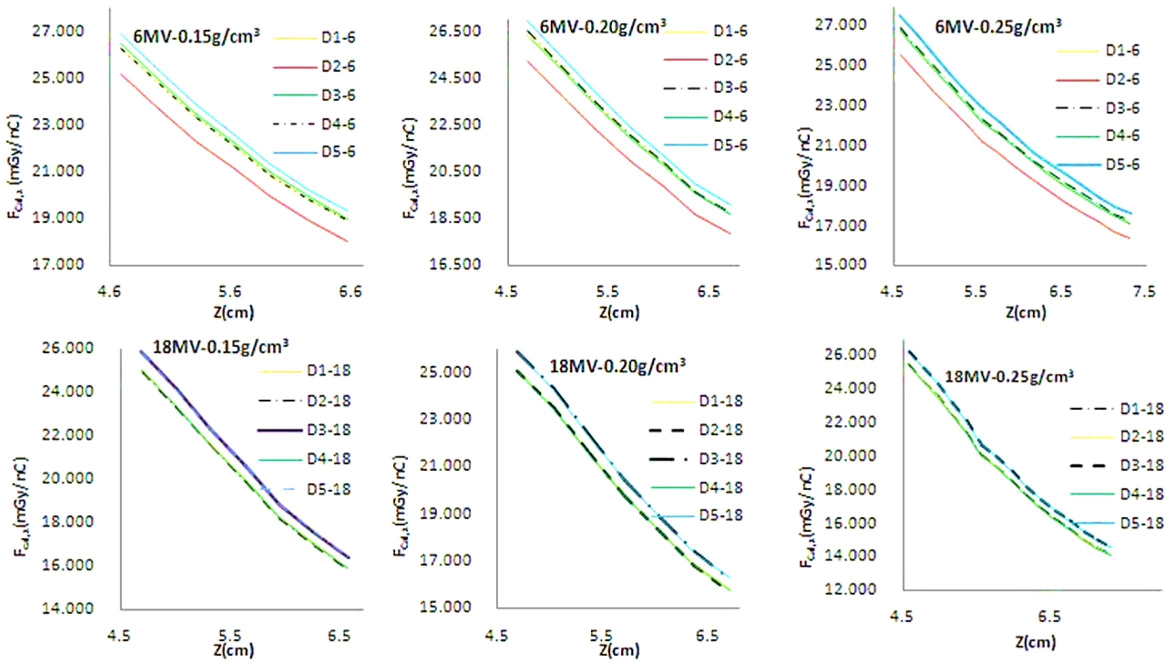

Figure 7. Diode calibration curves for 6-MV and 18-MV energies

Table 1. Deviations (%) between calculations and measurements for 6-MV and 18-MV energies

Density=0.15 g/cm^3										
Z_H (cm)	D1-6	D2-6	D3-6	D4-6	D5-6	D1-18	D2-18	D3-18	D4-18	D5-18
7	-0.70	-0.78	-1.09	-0.25	-0.36	-1.85	-1.61	-0.32	-1.20	-2.97
11	1.68	2.30	1.00	1.00	1.97	0.62	1.74	1.43	1.44	-0.05
15	-0.09	-0.80	-1.48	-0.30	-0.56	1.34	1.73	1.60	1.72	-0.14
Density=0.20 g/cm^3										
Z_H (cm)	D1-6	D2-6	D3-6	D4-6	D5-6	D1-18	D2-18	D3-18	D4-18	D5-18
7	1.43	2.44	0.52	1.85	2.29	-1.45	-1.67	-1.59	-0.79	-2.90
11	0.63	1.67	0.19	0.11	1.29	1.73	1.43	2.37	2.14	0.70
15	-0.14	0.40	-0.17	0.73	0.71	0.66	2.23	1.47	1.21	-0.46
Density=0.25 g/cm^3										
Z_H (cm)	D1-6	D2-6	D3-6	D4-6	D5-6	D1-18	D2-18	D3-18	D4-18	D5-18
7	0.76	-3.07	-0.08	0.28	0.41	-1.45	-1.45	-1.19	-1.66	-3.38
11	0.76	0.40	-0.03	1.45	-0.14	2.06	0.20	-0.90	3.01	-1.00
15	-0.60	0.11	-1.21	-0.70	-0.85	0.37	0.37	0.44	1.19	-0.73

Z_H: Total thickness from the surface of the phantom to the center of the insert

Table 2. Statistical quantities

Quantity	Deviation (%)	Dose (cGy)
Average	1.13	99.28
Average deviation	0.66	1.50
Standard deviation	0.80	1.95
95% CI	[0.97:1.29]	[98.88:99.68]
99% CI	[0.91:1.35]	[98.75:99.81]
99.9% CI	[0.85:1.41]	[98.61:99.96]

CI: Confidence levels at 95%, 99%, and 99.9%.

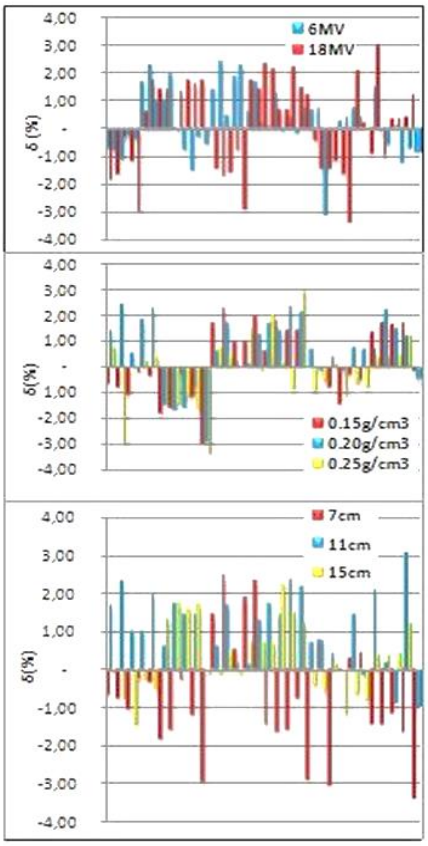

Figure 8. Histograms of deviations between measurements by comparison of two energy levels, three densities, and three depths.

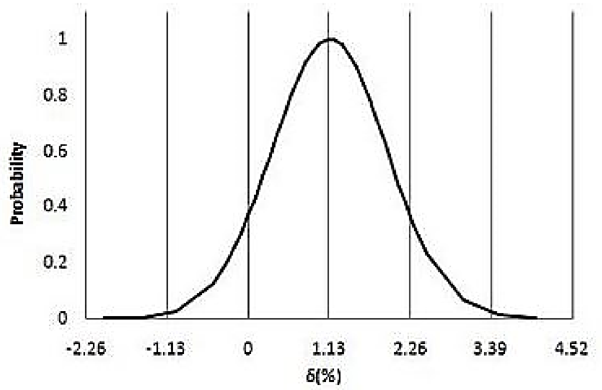

Figure 9. The Gaussian distribution of deviations

The obtained deviations remained in the order of magnitude around 2% and 3%, with a maximum value of 3.38% for 18-MV energies at a density of 0.25 g/cm^3 and depth of 7 cm and a minimum value of 0.03% for 6-MV energies at a density of 0.25 g/cm^3 and depth of 11 cm. Regarding the doses measured for 1 Gy, in all measurements, a maximum value of 1.04 Gy and a minimum value of 0.94 Gy were obtained.

Discussion

The evaluation of dose calculation algorithms in the presence of heterogeneity, besides the development of heterogeneous phantoms and/or virtual simulations using different materials, has always been an important subject of investigation [25-41]. The geometrical principle of heterogeneous phantoms with low density, whether they are made, simulated, or marketed, is the same, that is, based on the arrangement of a low-density layer sandwiched between the water-equivalent layers [26-28, 30-32, 35-41]. The goal is to simulate a heterogeneous environment to approximate the tissue architecture of pulmonary areas within the rib cage as much as possible. Cork is often used to simulate the low density of the lungs [25, 26, 28, 30, 35]; wood has been also examined [39]. In our study, the pulmonary region was simulated at three densities of 0.15, 0.20, and 0.25 g/cm^3, using layers and blocks of expanded polystyrene placed between the PMMA plates, with a supplement introducing a small cylindrical PMMA insert into the low-density region to simulate a tumor, thereby creating more heterogeneity.

The dose calculation in a heterogeneous environment is generally complex. Different algorithms have undergone improvements to optimize their calculation model and minimize the differences between calculations and treatment data of the machines. Their validation or evaluation is often based on a comparison of calculations with measurements of MC simulation, as reported in several studies [25-28, 30-37, 39-41]. Measurement is carried out with ionization chambers [26, 28-34, 40], films [25, 26, 28-30, 39], or thermoluminescent detectors (TLDs) [35].

In the present study, the AAA algorithm was evaluated by *in vivo* dosimetry with diodes; calibration was based on several measurement points, highlighting the calibration curves. A single measurement point at different depths was studied, corresponding to the dose at the center of the cylindrical insert. In a configuration similar to ours, Engelsman [3] measured the doses at three points inside a sphere simulating a tumor and at two points in the region of low density. Obviously, it would have been preferable to investigate several points in this study; this is one of the reasons why we continued this study (in progress) to determine the PDD instead of a single point.

Several studies have focused on the evaluation of AAA algorithm in heterogeneous media [25-35, 37-41]. However, the deviations between the algorithm calculations and measurements (and/or MC calculations) are not consistent in different studies. Bragg [26] obtained phantom deviations of 2.4% and 2.3%, respectively for energies of 6 MV and 10 MV at a depth of 10 cm for a field size of 10×10 cm^2 (maximum of -2.1% with the CIRS phantom for planning with several beams). Moreover, Tillikainen [27] reported deviations of less than 2% for several field sizes for 6-MV and 18-MV energies, using MC calculations as the reference; a maximum deviation of 8% was found for small fields. Also, the PDD curves for the field size of 10×10 cm^2 indicated a dose underestimation by the AAA algorithm after the enhancement region.

Van Esch [28] reported the good agreement of PDDs between the AAA calculations and measurements with the ionization chamber for two 6-MV and 18-MV energies in a field size of 10×10 cm^2, as well as for dose profiles. Comparison between the results obtained from AAA calculations and measurements with the films showed deviations of less than 5% with the CIRS phantom. In a recent study by Chopra [30] using several algorithms, including AAA for 6-MV energies, a good agreement (<3%) was found for PDDs and profiles in field sizes of 6×6, 12×12, and 24×24 cm^2 by comparing the AAA calculations with the measurements by the ionization chamber, films, and MC simulations.

Moreover, Rana [31] evaluated the AAA algorithm by carrying out measurements and calculations for three low-density gap thicknesses (2, 4, and 6 cm). Comparisons between the measurements and calculations in a field size of 10×10 cm^2 indicated deviations of more than 6%. The differences reported by Rosa [35] between the AAA calculations and measurements carried out by TLD showed that the PDD curves underestimated the doses after the enhancement zone. Besides, Singh [39] studied PDDs for 15-MV energies in a 10×10 cm^2 field and showed a good agreement between the AAA calculations and measurements with films and MC simulation.

Our results showed that a deviation of 45.6% represented a dose underestimation by the AAA algorithm, while a deviation of 54.4% indicated a dose overestimation. Moreover, Robinson [40] concluded that the AAA algorithm tended to overestimate the dose in low-density regions. Overall, evaluation of the AAA algorithm in a heterogeneous medium cannot be limited to a simple beam geometry, and deviations can be observed for more complex geometries (planning with several beams and small fields) or other conditions (respiratory movement and treatment planning with new techniques), as shown in some studies [25, 32, 33, 37, 39, 42].

The dose profiles showed that from a certain depth, the amplitude of the 6-MV beam curve became greater as compared to the 18-MV beam. This revealed that the dose collected at the end of the path increased by the dose accumulated by backscattered radiation. Low-energy photons produce a larger amount of divergent scatter [M5]. Indeed, the energy of an 18-MV beam is more penetrating, especially in a medium of low density; therefore, interactions with the medium at the end of the path become more important for energies of 6 MV. This backscattered radiation is often considered in equations involving the tissue phantom ratio (TPR) [14]. In this work, it was not necessary to introduce factors for dose calculations. The inversion of amplitude can be also caused by the anomalous scattering of X-rays, because after beam attenuation, the energy of photons approaches the absorption threshold of atoms in the medium.

The results did not show a significant diversion compared to the average value. An average value of 1.13% is generally expected to validate the dose calculation algorithm. For the three histograms, regardless of the comparison parameter, no significant difference was found. For these differences, we should consider the difficulty of manipulating diodes for posterior irradiation. Also, it is important to keep the same position of the phantom scanning instead of reversing its position. We tried to present all of the results and explain the differences observed in this study.

Conclusion

This study focused on the evaluation of the AAA algorithm using *in vivo* dosimetry by diodes. Besides, calibration of diodes was carried out in several depths of measurement, highlighting the calibration curves. The deviations between the calculations and the measurements remained within the recommended tolerance range for the evaluation of dose calculation algorithms in the presence of heterogeneity [24]. The calibration method based on dose profiles provided information about doses at depths outside d_{max} in a heterogeneous medium by relying on a single reading of the diode. Although the comparative curves of dose profiles showed an accumulation of backscattered radiation, integration of dose profiles in a heterogeneous medium for determining the calibration curves was sufficient to avoid complex formulae involving the TPR. This preliminary work also aimed to evaluate a dose calculation algorithm for more complex situations (in progress), especially by varying the geometry of phantoms, performing off-axis measurements, varying other parameters, such as field size and SSD, and including a multi-leaf collimator to establish a periodic verification protocol.

Acknowledgment

We would like to thank the Anti-Cancer Center of Blida, particularly the head of the department (Prof. K. Boualga).

References

1. Technical reports series N° 430. Commissioning and quality assurance of computerized planning systems for radiation treatment of cancer. International Atomic Energy Agency, Vienna. 2004.
2. Papanikolaou N, Battista JJ, Boyer AL, Kappas C, Klein E, Mackie TR, et al. Tissue inhomogeneity corrections for megavoltage photon beams. AAPM Task Group. 2004 Aug; 65:1-42.
3. Engelsman M, Damen EM, Koken PW, van′t Veld AA, van Ingen KM, Mijnheer BJ. Impact of simple tissue inhomogeneity correction algorithms on conformal radiotherapy of lung tumours. Radiotherapy and Oncology. 2001 Sep 1;60(3):299-309.
4. Ekstrand KE, Barnes WH. Pitfalls in the use of high energy X rays to treat tumors in the lung. Int J Radiat Oncol Biol Phys. 1990; 18:249-52.
5. Hunt MA, Desobry GE, Fowble B, Coia LR. Effect of low-density lateral interfaces on soft-tissue doses. Int J Radiat Oncol Biol Phys. 1997; 37:475-82.
6. Kornelsen RO, Young ME. Changes in the dose-profile of a 10 MV xray beam within and beyond low density material. Med Phys. 1982; 9:114-6.
7. Rice RK, Mijnheer BJ, Chin LM. Benchmark measurements for lung dose corrections for X-ray beams. Int J Radiat Oncol Biol Phys. 1988; 15:399-409.
8. Yorke E, Harisiadis L, Wessels B, Aghdam H, Altemus R. Dosimetric considerations in radiation therapy of coin lesions of the lung. Int J Radiat Oncol Biol Phys. 1996; 34:481-7.
9. Young ME, Kornelsen RO. Dose corrections for low-density tissue inhomogeneities and air channels for 10-MV x rays. Med Phys. 1983; 10:450-5.
10. Leunens G, van Dam J, Dutreix A, Van Der Schueren E. Quality assurance in radiotherapy by in vivo dosimetry. Entrance dose measurements, a reliable procedure. Radiother. Oncol. 1990; 17: 141–51.
11. Heukelom S, Lanson JH, Mijnheer BJ. Comparison of entrance and exit dose measurements using ionisation chambers and silicon diodes. Phys. Med. Biol. 1991; 36: 47–59.
12. Essers M, Keus R, Lanson J, Mijnheer B. Dosimetric control of conformal treatment of parotid gland tumours. Radiother. Oncol. 1994; 32: 154–62.
13. Van Dam J, Marinello G. Methods for in vivo dosimetry in external radiotherapy. Physics for clinical radiotherapy. ESTRO Booklet n. 1 (Garant). 1994.
14. Luca Cozzi, Antonella Fogliata-Cozzi. Quality assurance in radiation oncology. A study of feasibility and impact on action levels of an in vivo

dosimetry program during breast cancer irradiation. Radiotherapy and Oncology. 1998; 46: 29–36.

15. Technical reports series N° 398. Absorbed dose determination in external beam radiotherapy. An International Code of Practice for Dosimetry Based on Standards of Absorbed Dose to Water. International Atomic Energy Agency, Vienna, 2000.
16. User's Guide QEDTM Detector Model 1112 through 1116. Sun Nuclear corportation. Document 1112011. 2005.
17. Shi J, Sanders TJ, Simon WE. Calculation of diode sensitivity as a function of accumulated electron beam dose. Med. Phys. 1995;22.
18. Heukelom S, Lanson JH, Mijnheer B. In vivo dosimetry during pelvic treatment. Radiother. Oncol. 1992; 25: 111–20.
19. Colussi VC, Beddar AS, Kinsella TJ, Sibata CH. In vivo dosimetry using a single diode for megavoltage photon beam radiotherapy: Implementation and response characterization. Journal of Applied Clinical Medical Physics. 2001 Sep;2(4):210-8.
20. Alecu R, Alecu M, Ochran TG. A method to improve the effectiveness of diode in vivo dosimetry. Medical physics. 1998 May;25(5):746-9.
21. Sievinen J, Ulmer W, Kaissl W. AAA photon dose calculation model in Eclipse. Palo Alto (CA): Varian Medical Systems. 2005;118:2894.
22. Sievinen J, Ulmer W, Kaissl W. AAA photon dose calculation model in Eclipse. Palo Alto (CA): Varian Medical Systems. 2005;118: 2894.
23. Aarup LR, Nahum AE, Zacharatou C, Juhler-Nottrup T, Knoos T, Nystrom H, et al. The effect of different lung densities on the accuracy of various radiotherapy dose calculation methods: implications for tumour coverage. Radiother Oncol. 2009; 91:405–14.
24. Mijnheer B, Olszewska A, Fiorino C, Hartmann G, Knöös T, Rosenwald JC, et al. Quality assurance of treatment planning systems: practical examples for non-IMRT photon beams. Brussels: Estro; 2004.
25. Soh RC, Tay GH, Lew WS, Lee JC. A depth dose study between AAA and AXB algorithm against Monte Carlo simulation using AIP CT of a 4D dataset from a moving phantom. Reports of Practical Oncology & Radiotherapy. 2018 Sep 1;23(5):413-24.
26. Bragg CM, Conway J. Dosimetric verification of the anisotropic analytical algorithm for radiotherapy treatment planning. Radiotherapy and oncology. 2006 Dec 1;81(3):315-23.
27. Tillikainen L, Helminen H, Torsti T, Siljamäki S, Alakuijala J, Pyyry J, et al. A 3D pencil-beam-based superposition algorithm for photon dose calculation in heterogeneous media. Physics in Medicine & Biology. 2008 Jun 26;53(14):3821.
28. Van Esch A, Tillikainen L, Pyykkonen J, Tenhunen M, Helminen H, Siljamäki S, et al. Testing of the analytical anisotropic algorithm for photon dose calculation. Medical physics. 2006 Nov;33(11):4130-48.
29. Rønde HS, Hoffmann L. Validation of Varian's AAA algorithm with focus on lung treatments. Acta Oncologica. 2009 Jan 1;48(2):209-15.
30. Kashmiri L. Chopra, Paul Leo, Christopher Kabat, Durg Vijay Rai, Jaiteerth S, et al. Evaluation of dose calculation accuracy of treatment planning systems in the presence of tissue heterogeneities. Ther Radiol Oncol. 2018; 2:28.
31. Rana S, Rogers K. Dosimetric evaluation of Acuros XB dose calculation algorithm with measurements in predicting doses beyond different air gap thickness for smaller and larger field sizes. Journal of medical physics/Association of Medical Physicists of India. 2013 Jan;38(1):9.
32. Rana S, Rogers K, Pokharel S, Lee T, Reed D, Biggs C. Acuros XB algorithm vs. anisotropic analytical algorithm: A dosimetric study using heterogeneous phantom and computed tomography (CT) data sets of esophageal cancer patients. 2013.
33. Dubey S, Bagdare P, Kumar Ghosh S. Design and study of a heterogeneous cost effective thorax phantom for dosimetric evaluation of analytic anisotropic algorithm (AAA) and acuros XB algorithm (AXB). International Journal of Radiology & Radiation Therapy. 2020; 7(2).
34. Mohamed SA, Hassan GS, Elshahat KM. Evaluation of Calculation Algorithms for photon Beam dose in Heterogeneous Medium. Global Journal of Physics Vol. 2015 Jun 18;1(1).
35. Da Rosa LA, Cardoso SC, Campos LT, Alves VG, Batista DV, Facure A. Percentage depth dose evaluation in heterogeneous media using thermoluminescent dosimetry. Journal of applied clinical medical physics. 2010 Dec;11(1):117-27.
36. Fogliata A, Nicolini G, Clivio A, Vanetti E, Cozzi L. Dosimetric evaluation of Acuros XB Advanced Dose Calculation algorithm in heterogeneous media. Radiation oncology. 2011 Dec;6(1):1-5.
37. Zaman A, Kakakhel MB, Hussain A. A comparison of Monte Carlo, anisotropic analytical algorithm (AAA) and Acuros XB algorithms in assessing dosimetric perturbations during enhanced dynamic wedged radiotherapy deliveries in heterogeneous media. Journal of Radiotherapy in Practice. 2019 Mar 1;18(1):75-81.
38. Kim YL, Suh TS, Choe BY, Choi BO, Chung JB, Lee JW, et al. Dose distribution evaluation of various dose calculation algorithms in inhomogeneous media. International Journal of Radiation Research. 2016 Oct 1;14(4):269.
39. Singh N, Painuly NK, Chaudhari LN, Chairmadurai A, Verma T, Shrotiya D, et al. Evaluation of AAA and XVMC Algorithms for Dose Calculation in Lung Equivalent Heterogeneity in Photon Fields: A Comparison of Calculated Results with Measurements. J Biomed Phys Eng. 2018; 8(3).
40. Robinson D. Inhomogeneity correction and the analytic anisotropic algorithm. Journal of clinical medical physics. 2008; 9(2).
41. Gagné IM, Zavgorodni S. Evaluation of the analytical anisotropic algorithm in an extreme water–lung interface phantom using Monte Carlo dose calculations. Journal of Applied Clinical Medical Physics. 2007 Dec;8(1):33-46.
42. Hedin E, Bäck A, Chakarova R. Impact of lung density on the lung dose estimation for radiotherapy of breast cancer. Physics and Imaging in Radiation Oncology. 2017 Jul 1;3:5-10.